Materials Science and Engineering C 31 (2011) 452–457

Contents lists available at ScienceDirect

Materials Science and Engineering C

journal homepage: www.elsevier.com/locate/msec

Effects of temperature and torsion speed on torsional properties of single-walled carbon nanotubes

A.R. Khoei [a,*], E. Ban [a], P. Banihashemi [a], M.J. Abdolhosseini Qomi [b]

[a] Center of Excellence in Structural and Earthquake Engineering, Department of Civil Engineering, Sharif University of Technology, P.O. Box. 11365-9313, Tehran, Iran
[b] Department of Civil and Environmental Engineering, Massachusetts Institute of Technology, 77 Massachusetts Ave, 02139 Cambridge, USA

ARTICLE INFO

Article history:
Received 25 February 2010
Received in revised form 16 June 2010
Accepted 9 November 2010
Available online 4 December 2010

Keywords:
Carbon nanotube
Molecular dynamics
Temperature effect
Torsion speed
Torsional buckling

ABSTRACT

Carbon nanotubes (CNTs) are excellent candidates for torsional elements used in nanoelectro-mechanical systems (NEMS). Simulations show that after being twisted to a certain angle, they buckle and lose their mechanical strength. In this paper, classical molecular dynamics simulations are performed on single-walled carbon nanotubes (CNTs) to investigate the effects of torsion speed and temperature on CNT torsional properties. The AIREBO potential is employed to describe the bonded interactions between carbon atoms. The MD simulations clearly show that the buckling of CNTs in torsion is a reversible process, in which by unloading the buckled CNT in opposite direction, it returns to its original configuration. In addition, the numerical results reveal that the torsional shear modulus of CNTs increases by increasing the temperature and decreasing the torsion speed. Furthermore, the buckling torsion angle of CNTs increases by increasing the torsion speed and decreasing the temperature. Finally, it is observed that torsional properties of CNTs are highly affected by speed of twist and temperature of the nanotubes.

© 2010 Elsevier B.V. All rights reserved.

1. Introduction

CNTs are carbon nanotubes with nanometer diameters which have lengths up to micro-meters. Although this is not the way that they are produced, these structures can theoretically be considered as rolled graphene sheets. According to the direction in which the graphene sheet is rolled up, the resulting CNT can be zigzag, armchair, or chiral. In zigzag CNTs, a zigzag pattern is used for atoms in circumferential direction of the tube. In armchair tubes, this pattern is similar to the arm of a chair, and in chiral CNTs there is no specific circumferential pattern [1]. The first discovered CNTs were made up of several concentric rolled graphene sheets [2], but recent CNTs are produced by consisting of one shell of atoms [3]. CNTs have several interesting mechanical, electrical and thermal properties. They have a Young modulus in terapascal range [4], depending on their chirality and diameter, they can be metallic or semiconductor, can also be used as reinforcing agents in composites [5], as hydrogen storage in fuel cells [6], and moreover they have applications in producing sensors [7], transistors [8], displaying devices [9], actuators [10], artificial muscles [11], and as a rotary bearing, they can be used to make nano-scale motors [12].

The mechanical properties of CNTs can be measured by performing experimental tests, such as the direct tension test [13], bending experiment [14], and torsion test [15], or performing numerical simulations on CNTs in tension [16], or torsion [17]. Basically, there are two distinct numerical approaches in the modeling of nano-scale systems, i.e. the discrete and continuous methods, which are based on the Newtonian, or quantum mechanical descriptions. In many cases, modeling the structure of a CNT by a uniform thin cylindrical shell can be useful, however — the simulation of nano-scale material using continuum based models has some limitations. For instance, Chang [18] illustrated that the properties of a chiral CNT in torsion depend on the direction of loading, which is in an obvious contrast with the common assumptions of modeling CNTs by shell theory. Furthermore, taking the advantage of multi-scale assumptions, the implementation of Cauchy–Born rule and its prevalent modifications are restricted. It was shown by Khoei et al. [19] and Aghaei et al. [20] that the general assumptions for relating atomistic information to continuum models are only valid up to a limiting amount of deformation. Incorporating a modified Morse potential, Xiao et al. [21] developed a molecular structural mechanics simulation that is able to model the CNTs' behavior in tension and torsion. Li and Chou [22] proposed a structural–mechanical model by defining the CNT as a structure consisting of the beams and nodes as the atoms and bonds, respectively, to predict the mechanical properties of CNTs such as the Young modulus of CNTs and graphene sheets. A molecular mechanics based finite element model was developed by Meo and Rossi [23] and Rossi and Meo [24] to predict the properties of SWCNTs with promising accuracy. The advantage of these methods is that they are based on the inter-atomic potentials, which are able to predict the mechanical response of material at the small size scales and are less computationally expensive than the MD method. Although continuum based models are promising means of simulating large systems of CNTs, they are not able to consider all

* Corresponding author. Tel.: +98 21 6600 5818; fax: +98 21 6601 4828.
E-mail address: arkhoei@sharif.edu (A.R. Khoei).

0928-4931/$ – see front matter © 2010 Elsevier B.V. All rights reserved.
doi:10.1016/j.msec.2010.11.002

complex details in atomic interactions. One of the most accurate approaches in modeling of CNT systems consisting of thousands of atoms is based on the molecular dynamics (MD) simulation. In this study, a series of MD simulations is performed to investigate the mechanical properties of CNTs, particularly the effects of torsion speed and temperature on CNTs torsional properties.

The MD simulation performed by Yakobson et al. [25] on tensile behavior of carbon nanotubes demonstrated that the yield strain of a CNT in tension increases by increasing the rate at which the CNT is stretched and decreases by increasing the temperature of CNT. It was shown by Wei et al. [26] that this behavior can be explained using the transition state theory. Zhang et al. [27] performed MD simulations to investigate the effect of strain rate on the compressive buckling behavior of CNTs. They found that by increasing the strain rate, the buckling force and displacement become larger, but the stiffness of the tube remains constant. Huang et al. [28] performed tension experiments on CNTs at 2000 °C and found that CNTs have superplastic behavior in such circumstance with the tensile strain of 280% before the breaking point. It is noteworthy to state that the maximum tensile strain obtained for a CNT at room temperature is about 6% [13]. The extra elongation due to superplastic behavior is in contrast with the trend that appears in lower temperatures and is due to the effect of atomic diffusion, kink formation and motion in high temperature, which can help the CNT heal from defects in tension and prevent formation of cracks and the local or overall failure of the CNT [28].

Dumitrica et al. [29] combined the effect of chirality, strain rate, and temperature to present a map for the breaking strain of CNTs in tension at different conditions. In this map, the breaking strain of a zigzag CNT is less than the breaking strain of an armchair CNT. It was shown by Belytschko et al. [30] that the breaking mechanism of a zigzag CNT is initiated by the formation of a crack about its cross-section, while the breaking mechanism of an armchair CNT is initiated by a bond rotation mechanism known as the Stone–Wales deformation [31]. In their tensile models, the strain rate and temperature can affect the breaking strain only if the breaking mechanism is initiated by bond rotation, and therefore they have no effect on the breaking strain of zigzag nanotubes. Based on the strain rate dependency of CNTs' yield strain in tension, it was observed that the difference between the yield strain obtained by the MD simulations and those evaluated by atomic force microscopy experiments is due to high strain rates used in MD simulations [26]. Since the total duration of MD simulation is in the range of nanoseconds, one must use a high strain rate to observe the yielding of CNT which leads to a higher yield strain.

The Brenner inter-atomic potential [32] was employed by Yakobson et al. [33] into MD simulations to investigate the torsional properties of CNTs. They found that the CNTs rotate uniformly under torsion and their cross-section remains circular until a specific angle, after this angle the CNT buckles and ripples from its longitudinal direction. Yu et al. [34] observed that after buckling the CNT, its cross-section collapses to a dumbbell like shape, and during this process atoms move in both circumferential and longitudinal directions. Jeong et al. [35] demonstrated that coupling the tension to torsion of CNTs increases the shear modulus and the critical torsional moment of CNTs. They also presented that the torsional stiffness of CNTs increases with the diameter of tube as $K \sim d_t^{2.99}$, in which d_t is the diameter of the SWCNT. They claimed that the torsional stiffness of tube decreases by increasing the length of CNTs, and buckling occurs at a higher angle and a lower torsional moment for longer tubes. Recently, Wang [36] performed MD simulations to illustrate that filling a SWCNT with C60 fullerenes can enhance the strength of system.

In the present paper, the molecular dynamics simulations are performed to investigate the effects of temperature and torsion speed on mechanical properties of CNTs in torsion. By unloading the buckled CNT in opposite direction, it has been shown that the buckling of CNTs is a reversible process. In what follows, the MD simulation methodology is first explained. The results of MD simulations are then presented and the behavior of CNT is discussed at different circumstances. The torsional shear modulus and buckling torsion angle of CNTs are finally investigated at various temperatures and torsional speeds.

2. Molecular dynamics simulation

Molecular dynamics (MD) can be used to model carbon nanotubes and to derive their mechanical properties [37]. In MD simulation, the internal force exerted to each atom is calculated based on the inter-atomic potential defining the interaction of particles. A time integration method can be used based on the explicit or implicit technique to derive the configuration of the system after a time step Δt, which must be in the range of femto-seconds. In order to perform the MD simulation in a canonical ensemble, the atomic system is connected to a heat bath to maintain a constant temperature. In this method, the force exerted on each atom is modified based on the instantaneous temperature of the system.

In this study, the AIREBO potential is employed, which is applicable for hydrocarbons [38]. This potential is an extended form of the Brenner second generation potential [39]. As the onset of torsional buckling is investigated here, the intramolecular portion of this potential is used and the nonbonded interactions are neglected. The intramolecular part of the AIREBO potential expresses the chemical binding energy of atoms, considering their pair-wise distances, the angle between two bonds, and the dihedral angle formed between two plains containing three connected bonds. Thus, the chemical binding energy of a system of carbon and hydrogen atoms is defined as

$$E^{REBO} = \frac{1}{2}\sum_i \sum_{j\neq i} \left[V^R\left(r_{ij}\right) + b_{ij}V^A\left(r_{ij}\right)\right] \tag{1}$$

in which the sum is over each pair of atoms that are nearest neighbors, r_{ij} is the scalar distance between the ith and jth atoms, V^R is the pair-wise repulsive potential energy, V^A denotes the pair-wise attractive potential energy between the ith and jth atoms, and b_{ij} is the bond order term for the ith and jth atoms, which is influenced by the configuration of their surrounding atoms. The aforementioned pair-wise terms are defined as

$$V^R\left(r_{ij}\right) = -w_{ij}\left(r_{ij}\right)\left(1 + \frac{Q_{ij}}{r_{ij}}\right)Ae^{-\alpha_{ij}r_{ij}} \tag{2}$$

$$V^A\left(r_{ij}\right) = -w_{ij}\left(r_{ij}\right)\sum_{n=1}^{3} B_{ij}^n e^{-\beta_{ij}^n r_{ij}} \tag{3}$$

where B_{ij}^n, β_{ij}^n, A, α_{ij} and Q_{ij} are constant parameters. In the above relations, n is a counter over a series of constant values and w_{ij} is a cut-off function defined as

$$\begin{aligned} w_{ij}(r) &= S'\left(t_c\left(r_{ij}\right)\right) \\ S'(t_c) &= \Theta(-t_c) + \Theta(t_c)\Theta(1-t_c)\frac{1}{2}[1+\cos(\pi t_c)] \\ t_c\left(r_{ij}\right) &= \frac{r_{ij}-r_{ij}^{min}}{r_{ij}^{max}-r_{ij}^{min}} \end{aligned} \tag{4}$$

where $S'(t_c)$ is a switching function, t_c is a scaling function, $\Theta(t_c)$ is the Heaviside step function, $r_{ij}^{\min}$ is a limiting distance in the AIREBO potential, in which the effect of potential starts to fade if the distance between two atoms exceeds this distance, and $r_{ij}^{\max}$ is the maximum considerable distance between two atoms by which they have effect on each other. This function limits the range of a covalent bond and smoothly switches off the potential when the distance of two atoms

exceeds $r_{ij}^{\max}$. In this case, the two atoms will not be considered as near neighbors. The bond order term can be defined as

$$b_{ij} = -\frac{1}{2}\left(p_{ij}^{\sigma\pi} + p_{ji}^{\sigma\pi}\right) + \pi_{ij}^{rc} + \pi_{ij}^{dh} \tag{5}$$

where the principal contribution to the bond order term $p_{ij}^{\sigma\pi}$ is defined as

$$p_{ij}^{\sigma\pi} = \left(1 + \sum_{k\neq i,j} w_{ik}(r_{ik}) g_i\left(\cos\theta_{jik}\right) e^{\lambda_{jik}} + P_{ij}\right)^{-1/2} \tag{6}$$

where g_i is a penalty function introduced to impose a cost on bonds of one atom, which are close to each other, and is defined as

$$g_c\left(\cos\theta_{jik}\right) = g_c^{(1)}\left(\cos\theta_{jik}\right) + S'\left(t_N\left(N_{ij}\right)\right)\left[g_c^{(2)}\left(\cos\theta_{jik}\right) - g_c^{(1)}\left(\cos\theta_{jik}\right)\right] \tag{7}$$

where θ_{jik} is the angle formed by the vectors r_{ji} and r_{ki}, and $S'(t_N(N_{ij}))$ is a function of the coordination of central atom. This function returns a value inclined to $g_c^{(1)}$ for covalent compounds with low coordination and a value inclined to $g_c^{(2)}$ for highly coordinated bulk materials, where both $g_c^{(1)}$ and $g_c^{(2)}$ are the fifth-order splines. The function S' is defined in Eq. (4) and $t_N(N_{ij})$ is given as

$$t_N\left(N_{ij}\right) = \frac{N_{ij} - N_{ij}^{min}}{N_{ij}^{max} - N_{ij}^{min}} \tag{8}$$

where $N_{ij}^{\min}$ and $N_{ij}^{\max}$ are constant values for the scaling function. In Relation (6), $e^{\lambda_{jik}}$ is a function that improves the potential energy surface for the abstraction of hydrogen atoms from hydrocarbons, and P_{ij} is a two-dimensional cubic spline. In addition, π_{ij}^{rc} is a three-dimensional cubic spline which includes the contributions from radical and conjugation effects to the bond order term, and is a function of N_{ij}, N_{ji} and N_{ij}^{conj}, with N_{ij} and N_{ji} denoting the coordination numbers defined as

$$\begin{aligned} N_{ij} &= N_{ij}^{C} + N_{ij}^{H} \\ N_{ij}^{C} &= \left(\sum_{k\neq i} \delta_{kC} w_{ik}(r_{ik})\right) - \delta_{jC} w_{ij}\left(r_{ij}\right) \end{aligned} \tag{9}$$

where δ represents the Kronecker delta for two atoms, and N_{ij}^{conj} is the local measure of conjugation in the i–j bond defined as

$$\begin{aligned} N_{ij}^{conj} = 1 &+ \left(\sum_{k\neq i,j} \delta_{kC} w_{ik}(r_{ik}) S'\left(t^{conj}(N_{ki})\right)\right)^2 \\ &+ \left(\sum_{l\neq i,j} \delta_{lC} w_{jl}\left(r_{jl}\right) S'\left(t^{conj}\left(N_{lj}\right)\right)\right)^2 \end{aligned} \tag{10}$$

and $t^{conj}\left(N_{lj}\right)$ is defined as

$$t^{conj}(N) = \frac{N - N^{min}}{N^{max} - N^{min}} \tag{11}$$

The remaining contribution to the bond order term is π_{ji}^{dh}, which imposes a penalty for rotation around the multiple bounds defined as

$$\begin{aligned} \pi_{ji}^{dh} = T_{ij}\left(N_{ij}, N_{ji}, N_{ij}^{conj}\right) \sum_{k\neq i,j} \sum_{l\neq i,j} \\ \times\left[\left(1 - cos^2 w_{kijl}\right) w'_{ik}(r_{ik}) w'_{jl}\left(r_{jl}\right) \times \Theta\left(sin\left(\theta_{jik}\right) - s^{min}\right)\Theta\left(sin\left(\theta_{ijl}\right) - s^{min}\right)\right] \end{aligned} \tag{12}$$

where $s^{\min}$ is a constant, T_{ij} is another three-dimensional cubic spline, and w_{kijl} is the dihedral angle formed by the three bonds, i.e.

$$cos\left(w_{kijl}\right) = \frac{r_{ji} \times r_{ik}}{|r_{ji} \times r_{ik}|} \cdot \frac{r_{ij} \times r_{jl}}{|r_{ij} \times r_{jl}|} \tag{13}$$

By defining the bond-weighting function as

$$\begin{aligned} w'_{ij}\left(r_{ij}\right) &= S'\left(t'_c\left(r_{ij}\right)\right) \\ t'_c\left(r_{ij}\right) &= \frac{r_{ij} - r_{ij}^{min}}{r_{ij}^{'max} - r_{ij}^{min}} \end{aligned} \tag{14}$$

where $r_{ij}^{'\max}$ is a constant. Finally, the internal force exerted to each atom can be evaluated by taking derivative from the potential with respect to the position of each atom as

$$\mathbf{f}_m^{REBO} = -\nabla_m E^{REBO} = -\sum_i \sum_{j(>i)} \left[\nabla_m V^R\left(r_{ij}\right) + \left(\nabla_m \bar{b}_{ij}\right) V^A\left(r_{ij}\right) + \bar{b}_{ij} \nabla_m V^A\left(r_{ij}\right)\right] \tag{15}$$

where $\mathbf{f}_m^{REBO}$ is the force exerted to the mth atom in a system governed by the AIREBO potential.

In order to perform the simulation at constant temperature, the Berendsen thermostat [40] is employed here. By applying the Berendsen thermostat to the Velocity–Verlet time integration method, the position and velocity of atoms in the next step can be derived as

$$\begin{aligned} \mathbf{r}_i(t + \Delta t) &= \mathbf{r}_i(t) + \mathbf{v}_i(t)\Delta t + \frac{1}{2m_i}\Delta t^2 \mathbf{f}_i^{REBO}(t) \\ \mathbf{v}_i\left(t + \frac{1}{2}\Delta t\right) &= \mathbf{v}_i(t) + \frac{1}{2m_i}\Delta t \mathbf{f}_i^{REBO}(t) \\ T\left(t + \frac{1}{2}\Delta t\right) &= \left[\sum_i m_i \mathbf{v}_i^2\left(t + \frac{1}{2}\Delta t\right)\right] / 3Nk_B \\ \mu\left(t + \frac{1}{2}\Delta t\right) &= \gamma\left[1 - \frac{T_0}{T\left(t + \frac{1}{2}\Delta t\right)}\right] \\ \mathbf{v}_i(t + \Delta t) &= \frac{2}{2 + \mu\left(t + \frac{1}{2}\Delta t\right)\Delta t}\left[\mathbf{v}_i\left(t + \frac{1}{2}\Delta t\right) + \frac{1}{2m_i}\Delta t \mathbf{f}_i^{REBO}(t + \Delta t)\right] \\ \mathbf{f}_i^{REBO}(t + \Delta t) &= \mathbf{f}_i^{REBO}(t + \Delta t) - m_i \mu\left(t + \frac{1}{2}\Delta t\right)\mathbf{v}_i(t + \Delta t) \end{aligned} \tag{16}$$

where $\mathbf{r}_i$, $\mathbf{v}_i$ and m_i are the coordinate, velocity and mass of the ith atom. In above relations, t is the time elapsed from the start of simulation, $\mathbf{f}_i^{REBO}$ is the force modified by the Berendsen thermostat and T is the instantaneous temperature of the system. N is the number of particles in system, Δt is the time step, T_0 is the reference temperature, γ is the constant factor of the Berendsen thermostat, and k_B is the Boltzmann constant.

3. Numerical simulation results

In order to investigate the effects of temperature and torsion speed on mechanical properties of CNTs in torsion, a set of molecular dynamics simulations are performed. The numerical simulations are performed using four different SWCNTs, including: a 99.77 Å long (10,10) armchair, a (17,0) zigzag and a (15,15) SWCNT using two different lengths of 99.77 Å and 149.65 Å long (10,10) nanotube. In all MD simulations, a time step of 0.2 fs is generally used except in the case of high strain rate, or high temperature, in which lower time steps in the range of 0.05 fs are necessary that makes the computational simulation more expensive. At the initial stage of each simulation the nanotube structure is relaxed for

2 ps to obtain a state of equilibrium before starting the deformation process. After that by fixing two rows of atoms in one end, two rows of atoms on the other end of nanotube are then rotated. The displacement control technique is used together with a constant rotation speed for each simulation. For those simulations with constant temperature, a temperature of 300 K is maintained as the reference temperature, and for those simulations with constant rotation speed, a rotation speed of 10 GigaRad/s is employed. In order to perform the twist of 10 GigaRad/s, all constrained atoms are rotated by 0.001 rad per 5000 steps. It is observed that the equilibrium condition is obtained for nanotubes after this relaxation period. Carbon nanotubes studied here are twisted at 5 different temperature and twist speeds.

In Fig. 1, the variations with torsion angle of the strain energy and torque are presented for the 99.77 Å long (10, 10) CNT at 300 K and the rotation speed of 10 GigaRad/s. The MD simulation indicates that for a twisted CNT before the buckling point, the internal moment of CNT increases almost linearly by increasing the rotation angle, however — it has small local fluctuations because of thermal vibrations, as noted in reference [41]. Obviously, the carbon atoms rotate uniformly around the circumference, and the cross-section of CNT remains circular with no particular distortion on the surface of CNT. According to the theory of linear elasticity of thin-walled cylinders [42] and considering the Hook's law, the strain energy can be related to the rotation angle as

$$U = \iint \sigma \; d\varepsilon \; dV = \frac{1}{2} G \int \gamma_{torsion}^2 dV = G\pi h R^3 \frac{\theta^2}{L} \tag{17}$$

where U is the strain energy, σ and ε are the stress and strain, G is the torsional shear modulus, γ_{torsion} is the torsional shear strain, V is the volume, h is the thickness, R is the radius, θ is the torsional angle, and L is the length of CNT. The torsional stiffness of CNT can be expressed as

$$K = L\frac{d^2U}{d\theta^2} = L\frac{dT}{d\theta} = 2G\pi h R^3 \tag{18}$$

where T is the torque in the CNT which is related to the strain energy by

$$T = \frac{dU}{d\theta} \tag{19}$$

In order to compute the shear modulus of CNTs, the wall thickness of 3.4 Å is assumed, which is the interlayer distance in graphite and is a common assumption for the effective wall thickness of SWCNTs [13,15,18]. Considering the initial stages of potential energy curve

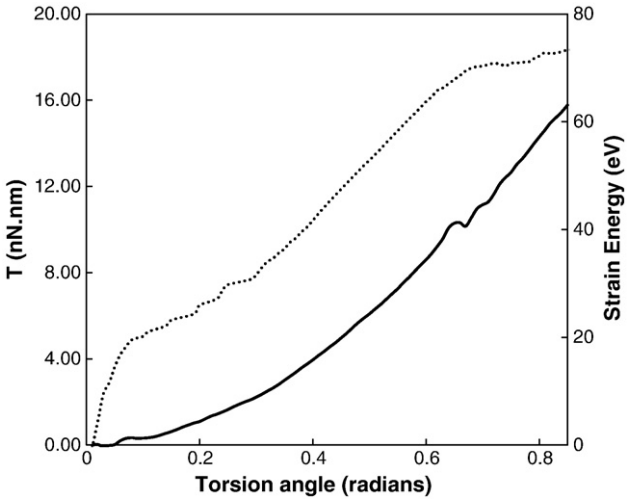

Fig. 1. The variations with torsion angle of the strain energy (solid curve) and torque (dotted curve) of the 99.77 Å long (10, 10) CNT at 300 K and 10 GigaRad/s.

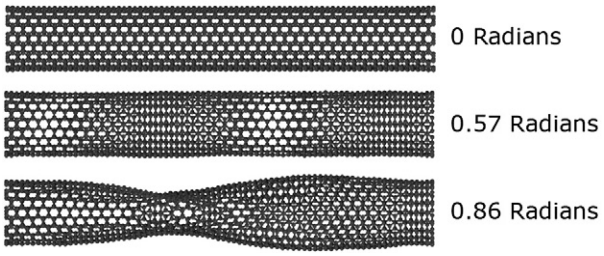

Fig. 2. The MD snapshots of a 99.77 Å (10,10) CNT in torsion at different torsion angles.

depicted in Fig. 1 together with Eq. (18) the shear modulus of CNT at 300 K subjected to the torsion speed of 10 GigaRad/s can be obtained as 394 GPa. This value is in the range of 410 ± 360 GPa reported experimentally by Hall et al. [15], and close to the value of 457 GPa obtained by Lu [43] using an empirical force constant model. Basically, it is observed that by twisting the tube more than a specific angle, the tube becomes unstable, its surface collapses, and the atoms make a sudden movement along the axis and in the circumferential direction of CNT. The snapshots of the 99.77 Å long (10,10) nanotube in torsion are illustrated in Fig. 2. Obviously, the surface of nanotube deforms at a torsion angle of 0.86 rad, in which the trends of strain energy and torque are changed in the tube.

The MD simulations indicate that the shear moduli of CNTs decrease by increasing the twist speed and increase by increasing the temperature. In Fig. 3, the shear moduli of the CNTs are presented at various temperatures and torsion rates. In this figure, the simulations are performed at various temperatures for the torsion rate of 10 GigaRad/s and also, at various torsion rates for the temperature

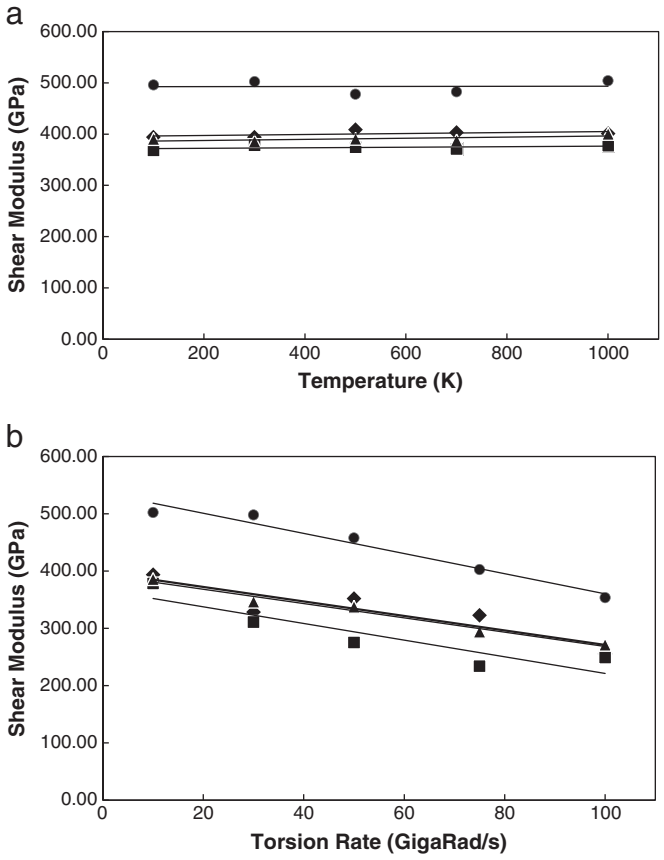

Fig. 3. The variations of shear modulus of the 99.77 Å long (10,10) (diamonds), (15,15) (squares), (17,0) (triangles), and the 149.65 Å long (10,10) (circles) nanotubes with (a) temperature, and (b) torsion speed.

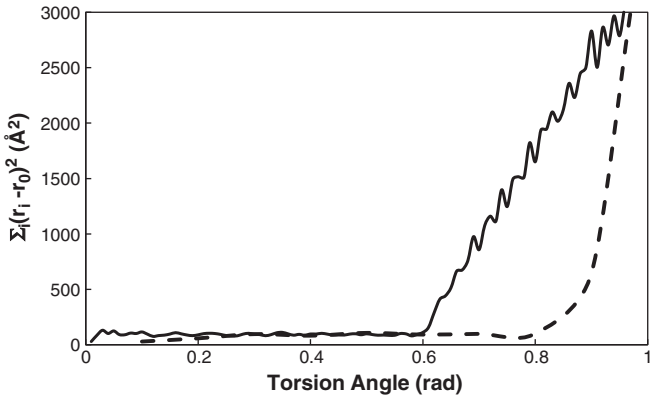

Fig. 4. The sum of squares of atoms radial displacements (SSARD) for CNTs in torsion at the torsion speed of 10 GigaRad/s (solid curve) and 100 GigaRad/s (dashed curve).

of 300 K. As can be observed, all four SWCNTs have almost similar behavior, in which the average shear moduli increases by 9 GPa due to increase of temperature from 100 K to 1000 K, and decreases by 143 GPa due to increase of torsion speed from 10 to 100 GigaRad/s.

In order to evaluate the buckling torsion angle, the sum of squares of atoms radial displacements (SSARD) is calculated by

$$SSARD = \sum_i (r_i - r_0)^2 \tag{20}$$

where r_i is the distance of ith atom from the CNT's axis and r_0 is the radius of measured CNT before loading. In Fig. 4, the variations with torsion angle of SSARD are plotted at torsion speeds of 10 and 100 GigaRad/s. As illustrated, the SSARD has small changes before the buckling point, which is due to thermal vibrations and the oscillations produced by rotation propagates along the CNT. Obviously, at a certain torsion angle the SSARD suddenly increases, which indicates the buckling angle of CNT, and at this stage the surface of CNT starts to deform. As shown in Fig. 4, the CNT rotated by the torsion speed of 10 GigaRad/s buckles earlier almost in 0.6 rad, while the CNT rotated by the torsion speed of 100 GigaRad/s buckles at almost 0.9 rad.

The variations with torsion speed of the buckling torsion angle and the buckling torque of CNTs are plotted in Fig. 5. Obviously, the twist angle and buckling torque can be affected by the torsion speed. As can be seen in this figure, the average buckling torsion angle for a nanotube twisted by a torsion speed of 100 GigaRad/s is almost 0.27 rad more than the buckling torsion angle for the torsion speed of 10 GigaRad/s, and the buckling torque is 1.34 (nN.nm) less for the rotation speed of 100 GigaRad/s. Considering the 99.77 Å (10,10) CNT rotated by 10 GigaRad/s at 100 K, the buckling happens at the torsion angle of 0.61 rad. By unloading the CNT in opposite direction from a twist angle of 0.5 rad, it can be seen that the CNT returns back to its original configuration, the strain energy and the SSARD return to their initial values, and the unloading path is identical to the loading path, as shown in Fig. 6. However, by unloading the rotated CNT from a twist angle of 0.7 rad, in which the buckling happens, it can be observed that although the CNT returns to its original configuration, it may not exactly pass through the same loading path. Thus, the torsional buckling of CNTs can be considered as a reversible process. In Fig. 6, the variations with torsion angle of the strain energy and the sum of squares of atoms radial displacements (SSARD) are plotted for a CNT twisted from relaxed state to 1 rad. Also plotted in this figure

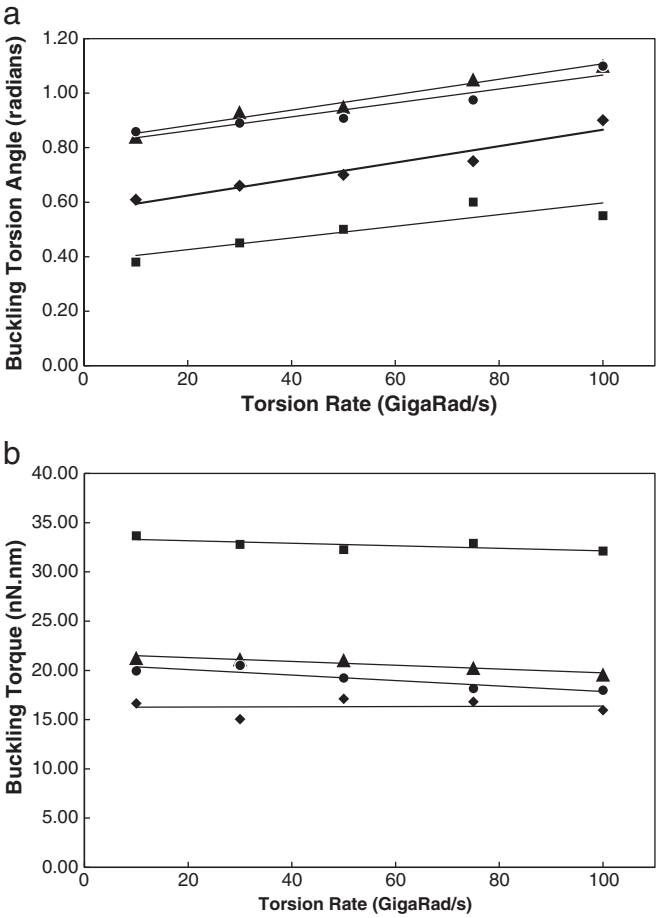

Fig. 5. The variations with torsion speed of (a) the buckling angle and, (b) the buckling torque for the 99.77 Å long (10,10) (diamonds), (15,15) (squares), (17,0) (triangles), and 149.65 Å long (10,10) (circles) nanotubes.

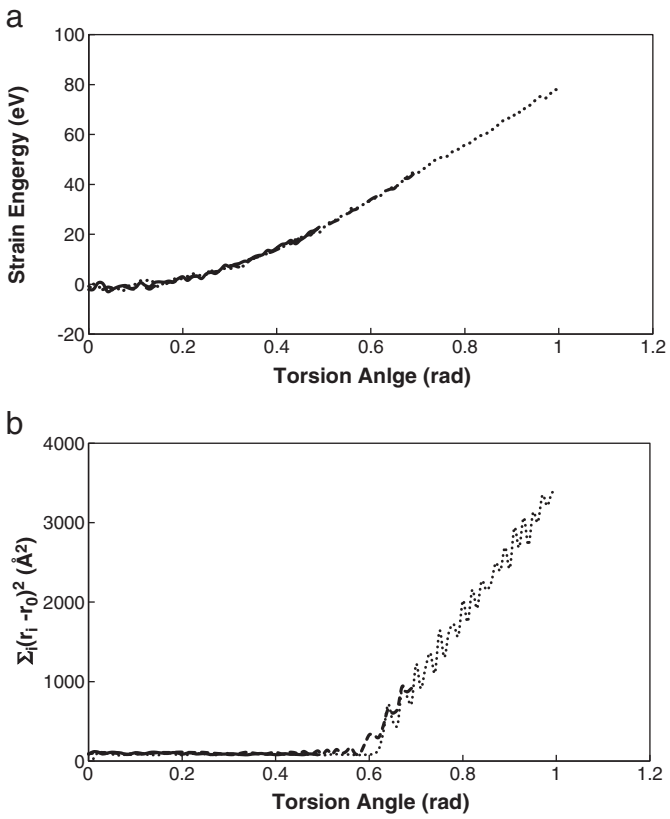

Fig. 6. The variations with torsion angle of (a) the strain energy, and (b) the sum of squares of atoms radial displacements (SSARD) for a CNT rotated from relaxed state to 1 rad (dotted curves), and unloaded in opposite direction from twist angle of 0.7 rad to relaxed state (dashed curves), and finally unloaded from torsion angle of 0.5 rad to relaxed state (solid curves).

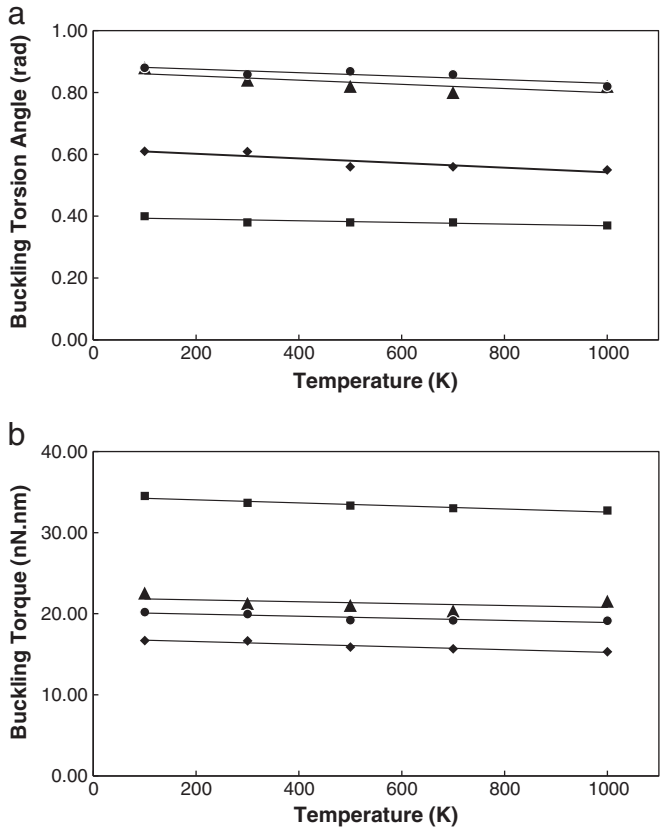

Fig. 7. The variations with temperature of (a) the buckling angle and, (b) the buckling torque for the 99.77 Å long (10,10) (diamonds), (15,15) (squares), (17,0) (triangles), and 149.65 Å long (10,10) (circles) nanotubes.

are the unloaded curves rotated in opposite direction from the angles of 0.5 and 0.6 rad to relaxed state. Finally, the variations of buckling torsion angle and buckling torque are plotted with temperature in Fig. 7. As can be seen, the buckling angle decreases by increasing the temperature, which can be due to the distortion of surface of the CNT at higher temperatures that can lead the CNT to an unstable state. By increasing the temperature from 100 K to 1000 K, the average buckling torsion angle decreases by 0.005 rad and the buckling torque increases by 1.32 (nN.nm).

4. Conclusion

In the present paper, the effect of strain rate and temperature was investigated on torsional properties of SWCNTs using molecular dynamics simulations. The AIREBO potential was employed to describe the bond interactions between the carbon atoms. A set of MD simulations was carried out at various temperatures and torsional speeds. It is shown that by increasing the temperature of nanotube both the buckling torsion angle and the buckling torque decrease but the shear modulus of nanotube increases. The molecular dynamics simulations indicate that the buckling of nanotube in torsion is very sensitive to the twist speed. In fact, by increasing the twist speed the buckling torque decreases and the buckling torsion angle increases dramatically, and as a result the shear modulus of nanotube decreases sharply with increasing the twist speed. Finally, it is shown that by unloading the buckled nanotube, the torsional buckling of CNTs is a reversible process.

Acknowledgements

Authors are grateful to Professor S.B. Sinnott from University of Florida for the helpful comments on MD simulation of CNTs, and also to S. Kadkhodaie from Sharif University of Technology in developing the CNT geometry generator. The authors are also grateful for the research support of the Iran National Science Foundation (INSF).

References

[1] R. Saito, G. Dresselhaus, M.S. Dresselhaus, Physical Properties of Carbon Nanotubes, Imperial College Press, 1998.
[2] S. Iijima, Nature 354 (1991) 56.
[3] S. Iijima, T. Ichihashi, Nature 363 (1993) 603.
[4] M.M.J. Treacy, T.W. Ebbesen, J.M. Gibson, Nature 381 (1996) 678.
[5] R. Andrews, C. Weisenberger, Solid States and Materials Science 8 (2004) 31.
[6] H.M. Cheng, Q.H. Yang, C. Liu, Carbon 39 (2001) 1447.
[7] S. Chopra, K. McGuire, N. Gothard, A.M. Rao, Applied Physics Letters 83 (2003) 2280.
[8] S.J. Tans, A.R.M. Verschueren, C. Dekker, Nature 393 (1998) 49.
[9] Q.H. Wang, A.A. Setlur, J.M. Lauerhaas, J.Y. Dai, E.W. Seelig, R.P.H. Chang, Applied Physics Letters 72 (1998) 2912.
[10] Y.H. Yun, V. Shanov, Y. Tu, M.J. Schulz, S. Yarmolenko, S. Neralla, J. Sankar, S. Subramaniam, Nano Letters 6 (2006) 689.
[11] U. Vohrer, I. Kolaric, M.H. Haque, S. Roth, U. Detlaff-Weglikowska, Carbon 42 (2004) 1159.
[12] A.M. Fennimore, T.D. Yuzvinsky, W.Q. Han, M.S. Fuhrer, J. Cumings, A. Zettl, Nature 424 (2003) 408.
[13] M.F. Yu, B.S. Files, S. Arepalli, R. Ruoff, Physical Review Letters 84 (2000) 5552.
[14] S. Iijima, The Journal of Chemical Physics 104 (1996) 2089.
[15] A.R. Hall, L. An, J. Liu, L. Vicci, M.R. Falvo, R. Superfine, S. Washburn, Physical Review Letters 96 (2006) 256102.
[16] C.F. Cornwell, L.T. Wille, Computational Materials Science 10 (1998) 42.
[17] B.W. Jeong, J.K. Lim, S.B. Sinnott, Journal of Applied Physics 101 (2007) 084309.
[18] T. Chang, Applied Physics Letters 90 (2007) 201910.
[19] A.R. Khoei, M.J. Abdolhosseini Qomi, M.T. Kazemi, A. Aghaei, Computational Materials Science 44 (2009) 999.
[20] A. Aghaei, M.J. Abdolhosseini Qomi, M.T. Kazemi, A.R. Khoei, International Journal of Solids and Structures 46 (2009) 1925.
[21] J.R. Xiao, B.A. Gama, J.W. Gillespie Jr., International Journal of Solids and Structures 42 (2005) 3075.
[22] C. Li, T. Chou, International Journal of Solids and Structures 40 (2003) 2487.
[23] M. Meo, M. Rossi, Materials Science and Engineering A 454–455 (2007) 170.
[24] M. Rossi, M. Meo, Composites Science and Technology 69 (2009) 1394.
[25] B.I. Yakobson, M.P. Campbell, C.J. Brabec, J. Bernholc, Computational Materials Science 8 (1997) 341.
[26] C. Wei, K. Cho, D. Srivastava, Physical Review B 67 (2003) 115407.
[27] Y.Y. Zhang, V.B.C. Tan, C.M. Wang, Carbon 45 (2007) 514.
[28] J.Y. Huang, S. Chen, Z.Q. Wang, K. Kampa, Y.M. Wang, S.H. Jo, G. Chen, M.S. Dresselhaus, Z.F. Ren, Nature 439 (2006) 281.
[29] T. Dumitrica, M. Hua, B.I. Yakobson, Proceedings of the National Academy of Sciences of the United States of America 103 (2006) 6105.
[30] T. Belytschko, S.P. Xiao, G.C. Schatz, R.S. Ruoff, Physical Review B 65 (2002) 235430.
[31] B.I. Yakobson, Applied Physics Letters 72 (1998) 918.
[32] D.W. Brenner, Physical Review B 42 (1990) 9458.
[33] B.I. Yakobson, C.J. Brabec, J. Bernholc, Physical Review Letters 76 (1996) 2511.
[34] W. Yu, W.X. Xi, N. Xianggui, Modeling and Simulation in Material Science and Engineering 12 (2004) 1099.
[35] B.W. Jeong, J.K. Lim, S.B. Sinnott, Applied Physics Letters 91 (2007) 093102.
[36] Q. Wang, Carbon 47 (2009) 507.
[37] D.C. Rapaport, The Art of Molecular Dynamics Simulation, Cambridge University Press, 1995.
[38] S. Stuart, A.B. Tutein, J.A. Harrison, The Journal of Chemical Physics 112 (2000) 6472.
[39] D.W. Brenner, O.A. Shenderova, J.A. Harrison, S.J. Stuart, B. Ni, S.B. Sinnott, Journal of Physics: Condensed Matter 14 (2002) 783.
[40] H.J.C. Berendsen, J.P.M. Postma, W.F. van Gunsteren, A. DiNola, J.R. Haak, The Journal of Chemical Physics 81 (1984) 3684.
[41] M. Endo, S. Iijima, M.S. Dresselhaus, Carbon Nanotubes, Elsevier Science, 1996.
[42] A.P. Boresi, R.J. Schmidt, O.M. Sidebottom, Advanced Mechanics of Materials, John Wiley, 1993.
[43] J.P. Lu, Physical Review Letters 79 (1997) 1297.